AFRL-PR-WP-TP-2006-254

SIMULATIONS OF CAVITY-STABILIZED FLAMES IN SUPERSONIC FLOW USING REDUCED CHEMICAL KINETIC MECHANISMS (POSTPRINT)

Jiwen Liu, Chung-Jen, Tianfeng Lu, and Chung K. Law

NOVEMBER 2005

Approved for public release; distribution is unlimited.

STINFO COPY

 This work was funded by Department of the Air Force contract FA8650-05-M-2616.

PROPULSION DIRECTORATE
AIR FORCE MATERIEL COMMAND
AIR FORCE RESEARCH LABORATORY
WRIGHT-PATTERSON AIR FORCE BASE, OH 45433-7251

REPORT DOCUMENTATION PAGE

Form Approved
OMB No. 0704-0188

1. REPORT DATE *(DD-MM-YY)*	2. REPORT TYPE	3. DATES COVERED *(From - To)*
November 2005	Conference Paper Postprint	09/21/2005 – 11/01/2005

4. TITLE AND SUBTITLE
SIMULATIONS OF CAVITY-STABILIZED FLAMES IN SUPERSONIC FLOW USING REDUCED CHEMICAL KINETIC MECHANISMS (POSTPRINT)

5a. CONTRACT NUMBER
FA8650-05-M-2616

5b. GRANT NUMBER

5c. PROGRAM ELEMENT NUMBER
61102F

6. AUTHOR(S)
Jiwen Liu and Chung-Jen Tam (Taitech, Inc.)
Tianfeng Lu and Chung K. Law (Princeton University)

5d. PROJECT NUMBER
2308

5e. TASK NUMBER
AI

5f. WORK UNIT NUMBER
01

7. PERFORMING ORGANIZATION NAME(S) AND ADDRESS(ES)

Taitech, Inc.
Beavercreek, OH 45430

Princeton University
Department of Mechanical and Aerospace Engineering
Princeton, NJ 08544

8. PERFORMING ORGANIZATION REPORT NUMBER

9. SPONSORING/MONITORING AGENCY NAME(S) AND ADDRESS(ES)

Propulsion Directorate
Air Force Research Laboratory
Air Force Materiel Command
Wright-Patterson AFB, OH 45433-7251

10. SPONSORING/MONITORING AGENCY ACRONYM(S)
AFRL-PR-WP

11. SPONSORING/MONITORING AGENCY REPORT NUMBER(S)
AFRL-PR-WP-TP-2006-254

12. DISTRIBUTION/AVAILABILITY STATEMENT
Approved for public release; distribution is unlimited.

13. SUPPLEMENTARY NOTES
Conference paper postprint published in the Proceedings of the 42nd AIAA/ASME/SAE/ASEE Joint Propulsion Conference and Exhibit.

PAO case number: AFRL/WS 05-2528; Date cleared: 31 Oct 2005.

14. ABSTRACT

The VULCAN CFD code integrated with a reduced chemical kinetic mechanism was applied to simulate cavity-stabilized ethylene-air flames and to predict flame stability limits in supersonic flows based on an experimental study. A 15-step reduced kinetic mechanism for ethylene was systematically developed through skeletal reduction with a directed relation graph and time scale reduction based on quasi-steady state assumptions. The accuracy of the reduced kinetic mechanism and its implementation in the VULCAN code were demonstrated in an auto-ignition problem with a range of parameters. 3D simulations were then carried out for cavity-stabilized flames at different fuel flowrates and turbulent Schmidt numbers. For comparison with the performance of the present reduced mechanism, a 3- and a 10-step global kinetic model were applied to simulate the same cavity combustor, and the results show that the 15-step reduced model predicts experimental results much better than the 3- and 10-step models. The importance of including accurate chemical kinetics in CFD simulations is therefore demonstrated.

15. SUBJECT TERMS
Plasma enhanced combustion, ethylene, kinetics models, CFD chemistry models, reduced mechanism, reduced chemistry

16. SECURITY CLASSIFICATION OF:			17. LIMITATION OF ABSTRACT:	18. NUMBER OF PAGES	19a. NAME OF RESPONSIBLE PERSON (Monitor)
a. REPORT	b. ABSTRACT	c. THIS PAGE			Dr. Skip Williams
Unclassified	Unclassified	Unclassified	SAR	22	19b. TELEPHONE NUMBER *(Include Area Code)* N/A

Standard Form 298 (Rev. 8-98)
Prescribed by ANSI Std. Z39-18

42nd AIAA/ASME/SAE/ASEE Joint Propulsion Conference & Exhibit
9 - 12 July 2006, Sacramento, California

AIAA 2006-4862

Simulations of Cavity-stabilized Flames in Supersonic Flows Using Reduced Chemical Kinetic Mechanisms

Jiwen Liu* and Chung-Jen Tam†
Taitech, Inc., Beavercreek, OH 45430

Tianfeng Lu‡ and Chung K. Law§
Department of Mechanical and Aerospace Engineering, Princeton University, Princeton, NJ 08544

The VULCAN CFD code integrated with a reduced chemical kinetic mechanism was applied to simulate cavity-stabilized ethylene-air flames and to predict flame stability limits in supersonic flows based on an experimental study. A 15-step reduced kinetic mechanism for ethylene was systematically developed through skeletal reduction with a directed relation graph and time scale reduction based on quasi-steady state assumptions. The accuracy of the reduced kinetic mechanism and its implementation in the VULCAN code were demonstrated in an auto-ignition problem with a range of parameters. 3D simulations were then carried out for cavity-stabilized flames at different fuel flowrates and turbulent Schmidt numbers. For comparison with the performance of the present reduced mechanism, a 3- and a 10-step global kinetic model were applied to simulate the same cavity combustor, and the results show that the 15-step reduced model predicts experimental results much better than the 3- and 10-step models. The importance of including accurate chemical kinetics in CFD simulations is therefore demonstrated.

Nomenclature

M	=	Mach number
Pr_t	=	turbulent Prandtl number
r	=	immediate error
Sc_t	=	turbulent Schmidt number
ε	=	threshold value
ν	=	stoichiometric coefficient
τ_{ext}	=	extinction residence time
τ_{ign}	=	ignition delay time
φ	=	global equivalence ratio
ω	=	reaction rate

I. Introduction

The U.S. Air Force (USAF) has been the supporting the development of hydrocarbon-fueled scramjet engines via the HyTech Program since 1995.[1] A key issue that has been addressed in this program is the fuel and air mixing and flameholding. The mixing of fuel and air in an airbreathing engine becomes increasingly inefficient and flameholding becomes increasingly difficult at high velocities, due to the reduced flow residence time in the combustors and the flow compressibility, which adversely affects the mixing rate. Wall cavities are outstanding flameholders for scramjet combustors because they provide sufficient residence time for the flameholding of hydrocarbon fuels in a supersonic stream and also they involve low total pressure losses. In the last decade, the Air Force Research Laboratory's Propulsion Directorate, Aerospace Propulsion Division (AFRL/PRA) has been developing several modern direct-connect test facilities involving different types of cavity flameholders for

* Senior Research Scientist, Associate Fellow AIAA.

† Senior Research Scientist, Associate Fellow AIAA.

‡ Research Staff, Member AIAA.

§ Professor, Fellow AIAA.

hydrocarbon-fueled scramjet combustors. In an effort to develop robust flameholding schemes, flame stability studies have been receiving special attention from these facilities. For example, Mathur et al.[2] demonstrated the ability of cavity flameholders to stabilize hydrocarbon flames at flight Mach numbers between 4 and 6 over a wide range of combustor fuel-air equivalence ratios. Gruber et al.[3] provided limited data on the operating range of cavity-stabilized flames. Rasmussen, et al.[4] obtained stability limits in directly fueled cavity flameholders for different air mass flowrates, cavity geometries, fuel injection schemes, Mach numbers, and fuel types. Most of these fundamental researches used ethylene as a fuel, because it has short ignition delays, good energy yields, and is a key component of cracked endothermic fuels such as JP7. While most of the investigations focused on experimental studies, there has been little effort in numerical studies on the stability of hydrocarbon-fueled flames in cavity flameholders in supersonic airflows, primarily due to the inherent complexities in physics.

Flame stability limits are characterized with either the fuel lean or fuel rich blowout. Flame blowout is a highly transient phenomenon and is very sensitive to aerodynamic and thermodynamic conditions. For instance, blowout is generally abrupt as a result of the Arrhenius response of chemical kinetics in competition with the more gradual heat loss through fluid mixing. Therefore, it is crucial to incorporate accurate finite-rate chemistry in the form of either detailed or reduced mechanisms for accurate prediction of blowout, in that even a small or moderate uncertainty in chemical kinetic rates could lead to gross errors in the simulation results. However, detailed reaction mechanisms are typically too computationally demanding due to the large number of species and reactions required, as well as the stiffness induced by the vastly different time scales, which may span many orders of magnitudes, between the major species and the highly reactive radicals. As such, detailed chemistry is rarely included in complex 3D turbulent flame simulations even for the simplest hydrocarbons, such as ethylene, and even by using the latest supercomputers. To overcome this difficulty, extensive efforts have been made to develop reduced reaction mechanisms of smaller sizes and reduced stiffness, while still being sufficiently accurate. Reduced mechanisms are typically derived from validated detailed mechanisms at two levels, namely skeletal reduction, which eliminates unimportant reactions and species, and time scale reduction, which involves partial equilibrium and quasi-steady state (QSS) assumptions.

The objective of the current study is to simulate cavity-stabilized flames and to predict flame stability limits in supersonic flows using reduced chemical kinetic mechanisms based on an experimental study with the AFRL/PRA direct-connect cavity combustor facility. The experimental study focused on the stability of ethylene-fueled flames and the results were reported in Ref. 4. The reduced mechanism in the present study was developed using the directed relation graph (DRG) method for skeletal reduction and the computational singular perturbation (CSP) theory for QSS based time scale reduction.[5] This 15-step mechanism was integrated into VULCAN,[6] which is a specialized CFD code for the analysis of high speed turbulent reacting flows and has been widely adopted for simulations of scramjet engines. A brief review of the reduction methods and the resulting mechanism will be provided in the following section, followed by the description of VULCAN. The VULCAN code integrated with the reduced mechanism is first validated in an auto-ignition problem, and is then applied to simulate the AFRL/PRA cavity combustor at a selected test condition with different fuel flowrates and turbulent Schmidt numbers. In the end, to demonstrate the importance of using an accurate reduced kinetic model in the current simulation, two global kinetic models, with 3 and 10 steps respectively, will be also applied to the same cavity combustor, and the discrepancies among the results from the different models will be discussed.

II. Methodology for Mechanism Reduction

A. Skeletal reduction using directed relation graph

The skeletal reduction is to identify and eliminate unimportant reactions or species. The elimination of species is of primary interest for most combustion simulations involving a Jacobian matrix which scales quadratically with the number of species. The method of DRG was developed specifically for direct elimination of unimportant species by resolving species couplings through graph searching. In DRG, direct species coupling was defined by the relative immediate error induced to one species, say A, due to the elimination of another, say B:

$$r_{AB}=\frac{\sum_{i=1,l}|\nu_{A,i}\omega_i\delta_{Bi}|}{\sum_{i=1,l}|\nu_{A,i}\omega_i|},\quad \delta_{Bi}=\begin{cases}1, & \text{if the ith reaction involves species } B\\ 0, & \text{otherwise}\end{cases} \tag{1}$$

where the subscripts A and B indicate the species identity, i is the ith reaction, $\nu_{A,i}$ the stoichiometric coefficient of species A in the ith reaction, and ω the reaction rate. It is seen that the denominator consists of the contributions to species A from each reaction, and the numerator consists of all the terms involving species B in the denominator.

Therefore r_{AB} roughly describes the importance of species B to A. If the relative error r_{AB} is not small compared to a threshold value ε, the removal of species B from the skeletal mechanism immediately induces a non-negligible error in A, and if A is to be retained in the skeletal mechanism, B should also be retained for accurate evaluation of the reaction rate of A. This requirement of species A to B is denoted as $A \rightarrow B$.

Species can also be coupled indirectly through direct coupling with intermediate species. For example, if $A \rightarrow B$ and $B \rightarrow C$, then A requires C indirectly. The set of species required either directly or indirectly by species A is defined as the dependent set of A, and it is readily seen that if species A is to be retained in the skeletal mechanisms, so should be all the species in its dependent set.

A sample relation of DRG is shown in Fig. 1 in which vertices A, B … F correspond to the respective species. The arrow shows the direction of dependence of one species on another, with its width indicating the strength of the dependence. The starting vertex A is a major species in the mechanism. The skeletal species in Fig. 1 correspond to all the vertices reachable from the starting vertex. Graph searching methods such as deep first search can thus be exploited to efficiently find all the vertices reachable from the starting one. Species A, B and D are therefore identified as the species of the skeletal mechanism in the current example.

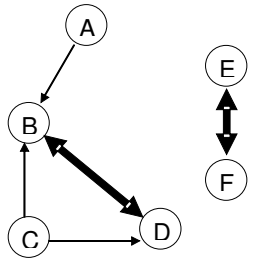

Figure 1. A DRG showing typical relations of the species.

To obtain a skeletal mechanism over a sufficiently wide range of parameters, such as pressure, temperature, equivalence ratio, and residence time, a set of reaction states are sampled from typical applications, such as perfectly stirred reactor (PSR) and auto-ignition. A local DRG reduction can be performed for each of these reaction states, and the union of the species sets of all the local skeletal mechanisms yields the species set of the global skeletal mechanism. Strictly speaking, the skeletal mechanism developed using DRG should only be applied to those applications and parametric spaces based on which it is developed. However, it is often the case that a skeletal mechanism developed from simple applications can be applied to more complicated simulations and still has satisfactory accuracy.[7]

B. Further reduction based on QSS assumptions

Since a skeletal mechanism contains only elementary reactions, it is applicable in the same manner as the detailed mechanism. However, the size of a skeletal mechanism is usually still too large for many demanding simulations. A further reduction can be accomplished by eliminating species with short time scales by approximating them to be in a steady state. The removal of the short time scales effectively reduces the stiffness of the system as well as the number of differential equations. This combined benefit usually dominates over the costs incurred by the internal algebraic iteration in solving the concentrations of the QSS species, and consequently results in an overall time saving in using QSS-based reduced mechanisms.

The short time scales can be identified by several methods and the CSP method was used in the present study. In this method, the time scales of independent modes are summed to an indicator weighed by sufficiently large radical pointers, the reciprocal of which can be defined as the time scale of the species. A critical time scale is selected to normalize the time scale of species, such that the time scale of the major species controlling the overall reaction rate of the system is normalized to unity. Species are considered to be QSS if their normalized time scales are smaller than a specified critical value. The selection of the critical time scale depends on the system. The extinction time for the PSR, and the auto-ignition time, can be respectively used as the characteristic time for extinction and ignition problems.

C. Mechanism reduction for ethylene

By applying the above methodology a reduced chemical kinetic mechanism was created for ethylene. The detailed ethylene oxidation mechanism used for reduction is from Qin et al.[8] and it consists of 70 species and 463 elementary reactions. For skeletal reduction, PSR and auto-ignition were used as the data source for reduction with pressure ranging from 0.1 ~ 30 atm, equivalence ratio from 0.7 ~ 1.3, initial temperature of 300 K for PSR and 1000 ~ 1800 K for auto-ignition, and residence time covering the entire ignition and extinction ranges. Data points were densely sampled over the above parametric space to ensure that all specific relations among the species can be represented by the sample set. During the graph searching, ethylene was selected as the starting species. By choosing the threshold accuracy value ε of 0.16, a skeletal mechanism consisting of 33 species was obtained. The species constituting this skeletal mechanism are: *H_2, H, O, O_2, OH, H_2O, HO_2, H_2O_2, C, CH, CH_2, CH_2*, CH_3, CH_4, CO, CO_2, HCO, CH_2O, CH_2OH, CH_3O, CH_3OH, C_2H_2, C_2H_3, C_2H_4, C_2H_5, HCCO, CH_2CO, CH_2CHO, n-C_3H_7, C_3H_6, α-C_3H_5, Ar, and N_2*. By eliminating all elementary reactions in the detailed mechanism which has any reactants or products not included in the above set of species, 205 elementary reactions were retained for the skeletal

mechanism.

The 33- species skeletal mechanism developed above was further reduced by using the CSP to identify the QSS species. By again using PSR and auto-ignition as the data bases, the time scale for each species was calculated for each data point, with their characteristic times being those of the extinction and ignition time respectively. The longest normalized time for each species was taken as the characteristic time scale for this species because it describes approximately its worst case characteristic time. A species is assumed to be a QSS species if its worst-case normalized time scale is shorter than the specified threshold value ε of 0.025. The QSS species identified were then removed from the skeletal mechanism and an internal algebraic loop was used to solve the concentrations of the QSS species. The final reduced mechanism consists of 19 species or 15 global steps. These 19 species are: H_2, H, O, O_2, OH, H_2O, HO_2, H_2O_2, CH_3, CH_4, CO, CO_2, $CH2O$, C_2H_2, C_2H_4, C_2H_6, CH_2CO, C_3H_6, and N_2.

III. VULCAN CFD Code

In this study the CFD code in which the above reduced kinetic mechanism was implemented is based on the VULCAN code. In contrast to most CFD codes, VULCAN has been developed from its inception to be an analysis tool for high-speed turbulent reacting flows. The VULCAN flow solver is presently being used in the USAF HyTech program as well as NASA hypersonic vehicle programs. In addition, VULCAN is also used by both industry and academic institutions. Ongoing development and maintenance of VULCAN is being performed by NASA Langley. Its development is primarily driven by application to high-speed propulsion devices.

VULCAN is a density-based CFD code applicable to complicated 2D and 3D geometries by using multiblock structured grid. Grid lines across a block interface can be continuous or discontinuous. The code solves the Reynolds-averaged Navier Stokes (RANS) equations appropriate for calorically or thermally perfect gases with a cell-centered finite volume scheme. The equation set can be integrated in a fully elliptic or space-marched manner. The inviscid fluxes can be evaluated with central differences, Roe's flux difference method, or a low-diffusion flux vector split scheme. Several flux limiters are provided to ensure total variation diminishing. A variety of two-equation turbulence models are available, along with one-equation and explicit algebraic Reynolds stress models. Assumed PDF options exist for modeling turbulence-chemistry interactions. Chemically reacting flows can be modeled with general finite-rate kinetics models. The code also contains full multi-grid capabilities, allowing rapid convergence for steady-state problems. For parallel computation, the MPI message passing library is used as a communication software in the code.

In the original VULCAN code the chemical kinetic models must be based on the standard Arrhenius equation and the reaction rate depends only on temperature. In reality, reaction rates may depend on pressure as well as temperature. In the present reduced kinetic mechanism of ethylene, either the Lindemann or Troe expression is applied to account for the pressure dependence in some reactions. In order to accommodate the pressure dependent reaction rate, the VULCAN code was modified by introducing a subroutine as a driver. This driver is called to provide flow information such as temperature, pressure, species concentrations, etc. every time before a reaction rate is computed. Introducing this driver leads to little change in the source code.

Turbulence modeling is one of the largest challenges in numerical analysis of turbulent reacting flows. In this study the turbulence model was based on the Menter turbulence model. The Menter model is essentially the standard high-Reynolds-number form of the Wilcox k-ω model near solid surfaces, but it smoothly transitions to a standard Jones-Launder k-ε model near the outer portion of the boundary layer and in regions of free shear. To relax the grid requirements near solid surfaces, the wall matching procedure of Wilcox was employed in all regions where the y+ of the first cell exceeds ten. At high speeds the flow compressibility effect may become important and it can lead to a reduced mixing rate. To account for this effect, a compressibility correction is normally introduced in turbulence models. However, all present compressibility correction models seem to do more harm than good in predictions for scramjet engine applications. Therefore, the compressibility correction was disabled in the present simulation. Also, in the RANS calculation, the turbulent transport of momentum is modeled by the eddy viscosity model while the turbulent transport of energy and mass is modeled using the gradient diffusion hypothesis. The diffusion rates for energy and mass are controlled by specifying the turbulent Prandtl (Pr_t) and Schmidt (Sc_t) numbers. Constant values for these numbers are usually assumed in applications, although their values have been found to vary spatially.[9, 10] Calculations performed by various authors[11, 12, 13] have shown strong sensitivity of the solution to these numbers, especially to Sc_t. Therefore, extreme care should be taken when attempting to characterize scramjet engines with constant turbulent transport coefficients. This is especially true for the present study because the turbulent mixing of fuel and air is one of the most important phenomena for conditions near blowout, and the value of Sc_t controls the extent of turbulent mixing. In this study, Pr_t and Sc_t were chosen to be 0.89 and 0.5, respectively, unless otherwise specified.

IV. Results and Discussion

A. Validation study

To demonstrate the accuracy of the reduced kinetic mechanism for ethylene and also the correctness of its implementation into the VULCAN code, a validation study was first carried out by employing the modified VULCAN code to predict the ignition delay time (τ_{ign}) for an auto-ignition problem using a range of initial

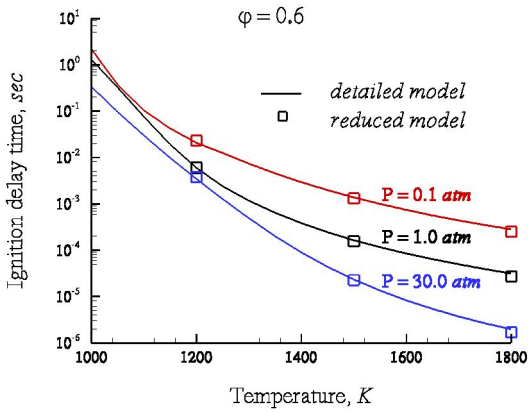

(a)

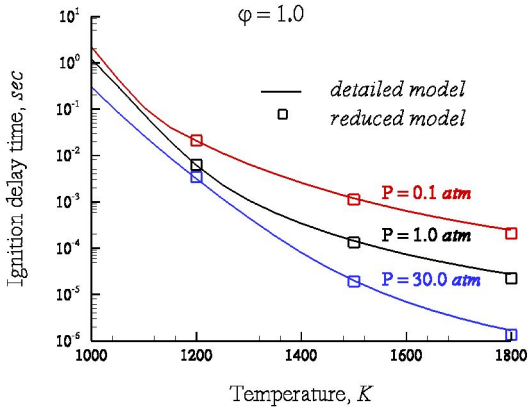

(b)

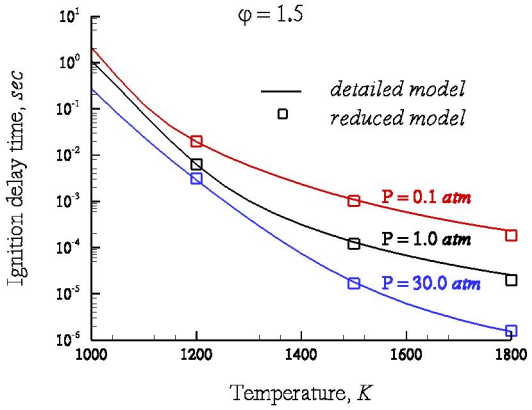

(c)

Figure 2. Comparisons of ignition delay time at the equivalence ratio of (a) φ=0.6, (b) φ=1.0, and (c) φ=1.5.

temperatures, pressures, and equivalence ratios. For this study, only a single grid cell was needed and the problem thus had constant volume. All simulations were conducted in the DOD ASC MSRC's SGI Origin 3900 machines. The time steps in the transient simulation strategy were different for different cases and they varied from 10^{-9} to 10^{-6} second. Temperature became steady between 5,000 and 50,000 steps and the runtime was less than 15 minutes. Figure 2 shows the comparisons of τ_{ign} between the 15-step reduced and detailed kinetic mechanism calculations for equivalence ratios of φ=0.6, 1.0., and 1.5. For a specific φ, a total of nine cases were considered for the reduced kinetic mechanism with initial temperatures of 1200 K, 1500 K, and 1800 K and initial pressures of 0.1 atm, 1.0 atm, and 30.0 atm. It is seen that the τ_{ign} from the reduced kinetic mechanism agrees very closely with that from the detailed one for the entire parameter range.

B. AFRL/PRA cavity combustor simulation with the 15-step reduced kinetic mechanism

AFRL/PRA direct-connect cavity combustor test rig features a facility nozzle, an isolator section, a cavity section, and a post-cavity section. Figure 3 shows half of the geometry configuration of this test rig. A close-up view of the cavity section is provided in Fig. 4. Room-temperature ethylene in the test was fed into the cavity from ten injectors placed on the cavity ramp wall. The air mass flowrate was varied by adjusting the plenum pressure upstream of the facility nozzle. At each test condition, the fuel flowrate was gradually increased until the cavity was ignited. Once the cavity was lit, the fuel flow was gradually decreased to the point where the cavity blew out. For the current numerical study, the selected inflow test condition was a Mach 2 flow with a total pressure and temperature of 414 kPa and 589 K, respectively. The incoming air mass flowrate was 3.1 kg/sec and the measured fuel flowrate at lean blowout was 0.46 kg/sec. This test datum will be used to validate the present numerical results.

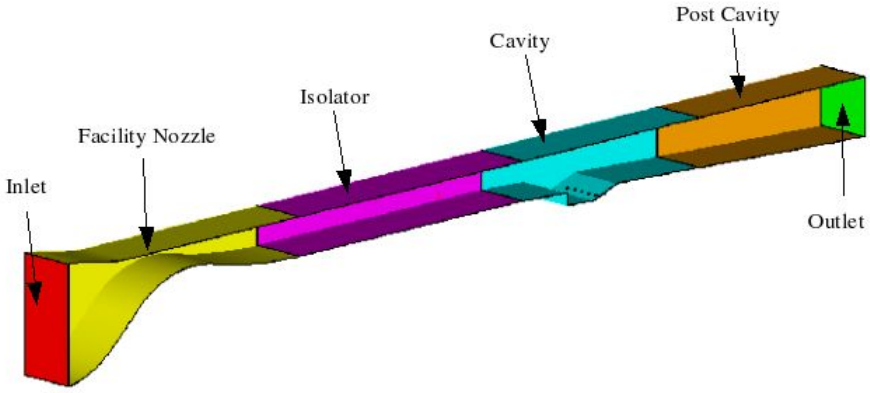

Figure 3. Geometric configuration of AFRL/PRA cavity combustor.

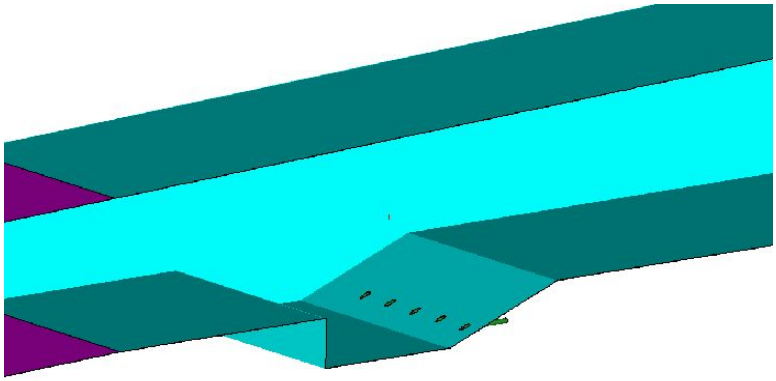

Figure 4. Close-up view of the cavity section.

In an effort to reduce the computational time required to perform the simulations without sacrificing grid resolution, the existence of symmetry planes between adjacent fuel injectors was presumed. This approximation is rigorously correct in the limit of an infinite array of injectors where the combustor side walls are non-existent. With this presumption, only a slice of the combustor facility with a half injector was needed in the modeling. Figure 5 shows the computational domain used for the AFRL/PRA combustor simulation. The total grid size is about one million. Figure 6 shows a close-up view of the grid in the cavity region with the injector tube. In order to check the performance of the reduced kinetic model and also examine the flame stability limits, simulations with different fuel flowrates were carried out in this study. The lean blowout case with a fuel flowrate of 0.46 kg/sec was considered as the baseline case. Three more cases with fuel flowrates of 4, 5, and 10 times the baseline flowrate were investigated and they are labeled as the 4X, 5X, and 10X cases, respectively, in the following discussion. These four cases with different fuel flowrates cover combustion from the fuel-lean to fuel-rich conditions.

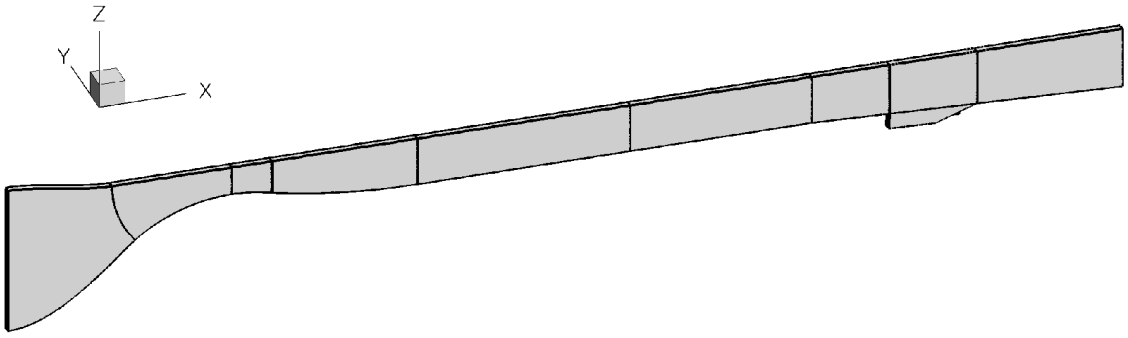

Figure 5. Computational domain for the ARFL/PRA cavity combustor.

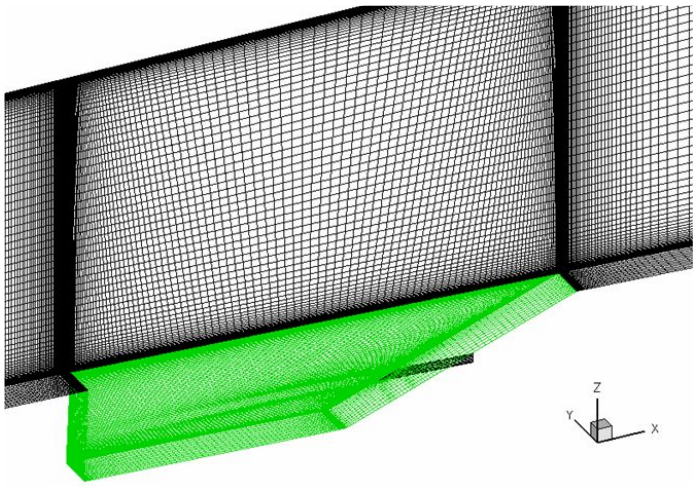

Figure 6. Close-up view of the grid in the cavity section.

AFRL/PRA cavity combustor was designed to study lean and rich flame blowout only in the cavity and it was not intended to achieve sustained combustion in the core flow. Therefore, a change of fuel flowrate has an impact only on the flow in the cavity region. Thus, to further reduce the computational cost, the computational domain in Fig. 5 was broken into two separate regions, with one containing the facility nozzle and another containing the isolator and cavity combustor. The simulation in the facility nozzle domain was conducted first. The flow profile at the exit plane from this simulation was then saved and used as the inflow condition for the simulation containing the domain comprised of isolator and cavity combustor. The simulation for the facility nozzle needs to be redone only when different air inflow conditions are used. Due to the still relatively large computational load, 16 parallel

processors were used for each simulation and they were from the DOD ASC MSRC's SGI Origin 3900 or Compaq Sc-45 machines. For a run with combustion, ignition was achieved by introducing an ignition source in the cavity region. This source was removed after several hundred flow solver iterations. All solutions reached steady state and their mass conservation errors were controlled below 0.1%. Except for the initial stage of the solution process, the CFL number was usually set to be 4 or 5. For the cases with very small fuel flowrates in the injector, the CFL number had to be reduced to 1 or 2.

Figures 7, 8, 9, and 10 show the local equivalence ratio, temperature, and CO_2 mass fraction contours at the baseline, 4X, 5X, and 10 X cases, respectively. The surfaces where the contours are shown include the cavity wall, injector wall, and the symmetry plane across the injector. To help in the result analysis, the stoichiometric lines are also plotted for each contour and they are represented as the white lines. For the baseline case (Fig. 7), fuel in the injector is not choked and it is injected into the cavity at very low speed (M≈0.1). Except in the region close to the injector port, the cavity is filled with air as seen in Fig. 7(a). Under such a fuel-lean condition, the present study predicted blowout, which is consistent with the experimental observation. The temperature in the cavity is found to be approximately equal to the total temperature (= 589 K) of the incoming air flow. Due to the flameout, the combustion product CO_2 is not present in the cavity region (Fig. 7(c)).

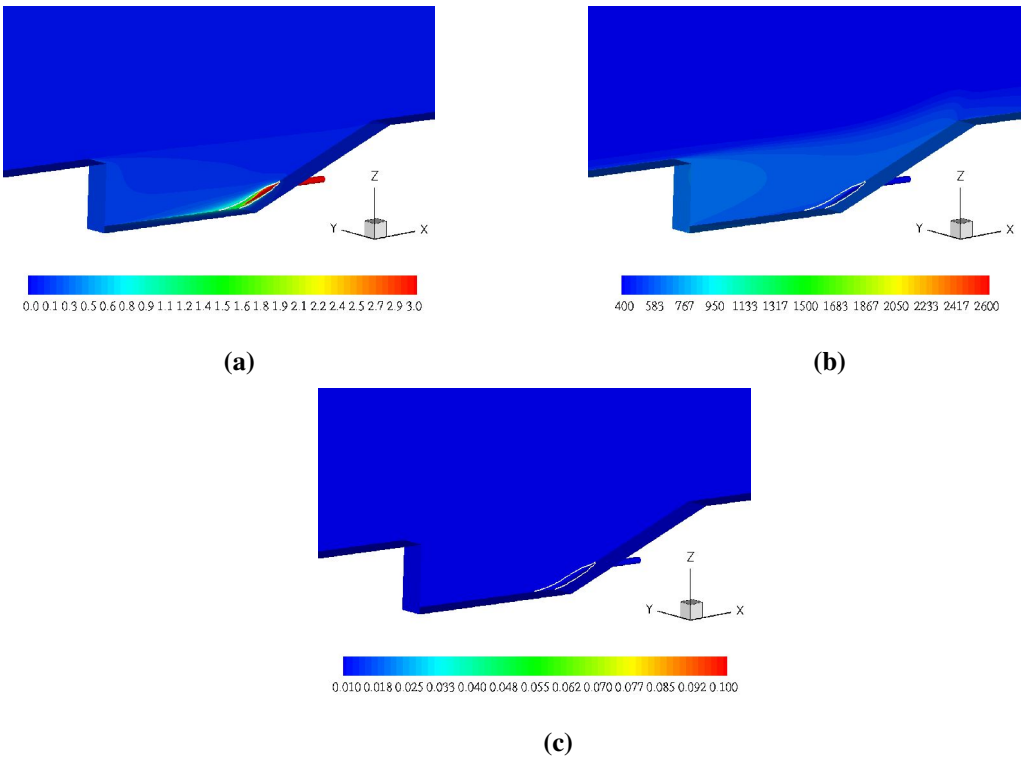

Figure 7. Contours of (a) local equivalence ratio, (b) temperature, and (c) CO_2 fraction for the baseline case.

For the 4X case (Fig. 8), the fuel flowrate is increased to be four times higher and the fuel is recirculated into most of the cavity region, as seen in Fig. 8(a). The cavity flow is usually characterized by a shear layer and a recirculation zone. On the symmetry plane, the stoichiometric line lies inside the shear layer, which separates the recirculation zone and the outer freestream of air. The flow near the cavity wall is found to be fuel rich (red color). Due to the extensive mixing of fuel and air, sustained combustion was predicted and the flame was stabilized in the cavity center region, including parts of the shear layer and the recirculation zone, as shown in Fig. 8(b). In addition to temperature, CO_2 may also be used as an indicator of combustion intensity. However, under fuel-rich or high flame temperature condition, CO_2 dissociates into CO and its amount is reduced. As a result, a high CO_2 mass fraction is observed near the stoichiometric line instead of in the region where the peak flame temperature is located (Fig. 8(c)).

As the fuel amount is further increased to five times higher than that of the baseline case (Fig. 9), the flow in the recirculation zone becomes more fuel rich and it pushes the stoichiometric line upward, especially in the ramped aft wall region, as seen in Fig. 9(a). Consequently, the flame region also moves to the aft wall (Fig. 9(b)). Due to the

intensified fuel-rich condition, combustion in the center of the recirculation zone becomes weak and the corresponding flow temperature is reduced. As in the 4X case, CO_2 is produced mainly near the vicinity of the stoichiometric line with a local equivalence ratio less than 2 as shown in Fig. 9(c).

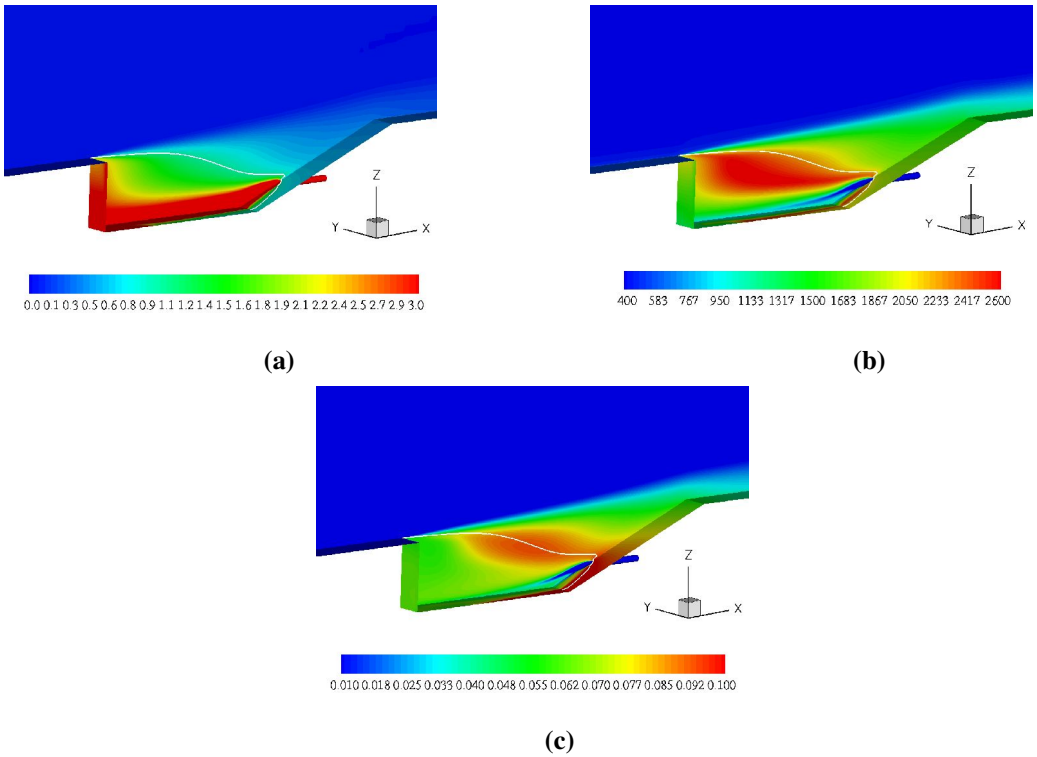

(a) **(b)**

(c)

Figure 8. Contours of (a) local equivalence ratio, (b) temperature, and (c) CO_2 mass fraction for the 4X case.

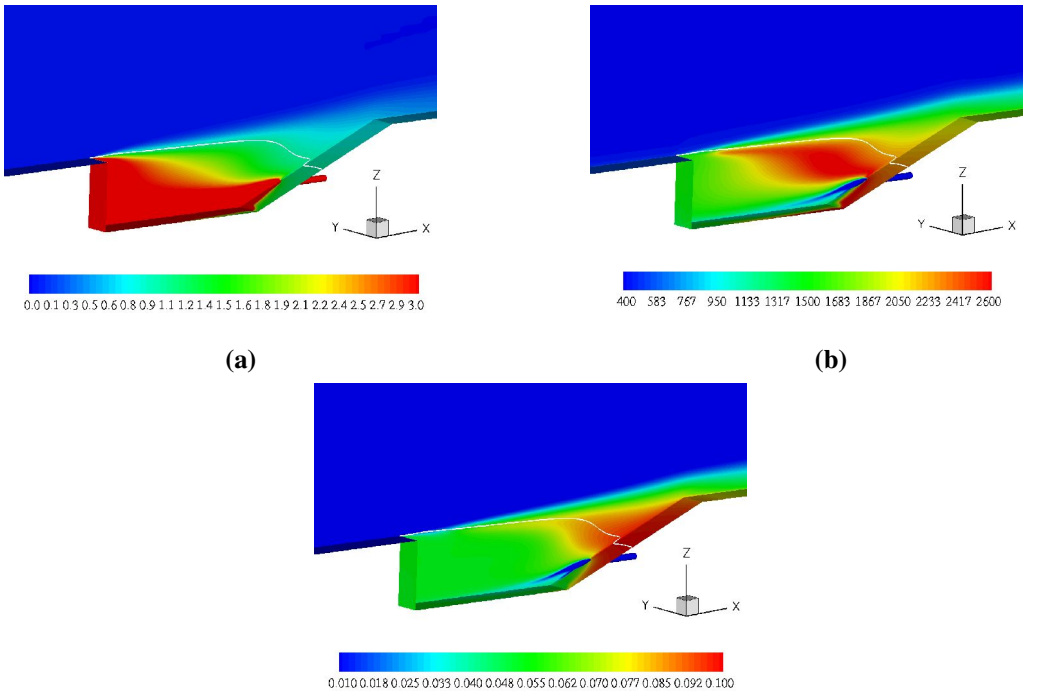

(a) **(b)**

(c)

Figure 9. Contours of (a) local equivalence ratio, (b) temperature, and (c) CO_2 mass fraction for the 5X case.

Figure 10 provides the contours for the fuel flowrate of ten times higher than that of the baseline case. At this condition most of the cavity is flooded with fuel and the stoichiometric line is pushed into the higher velocity region near the freestream at the top of the cavity (Fig. 10(a)). The flame remains lit but it is contained in a small region near the ramped aft wall and surrounded by the fuel-rich flow on the left and high-speed freestream on the top as seen in Fig. 10(b). It is expected that a further increase of the fuel flowrate would result in an even smaller flame region and colder recirculation zone, eventually leading to fuel-rich blowout. The clearly diminishing combustion for the 10X case is also revealed by the CO_2 contour in Fig. 10(c); the pronounced CO_2 is now only found in a region near the upper portion of the aft wall.

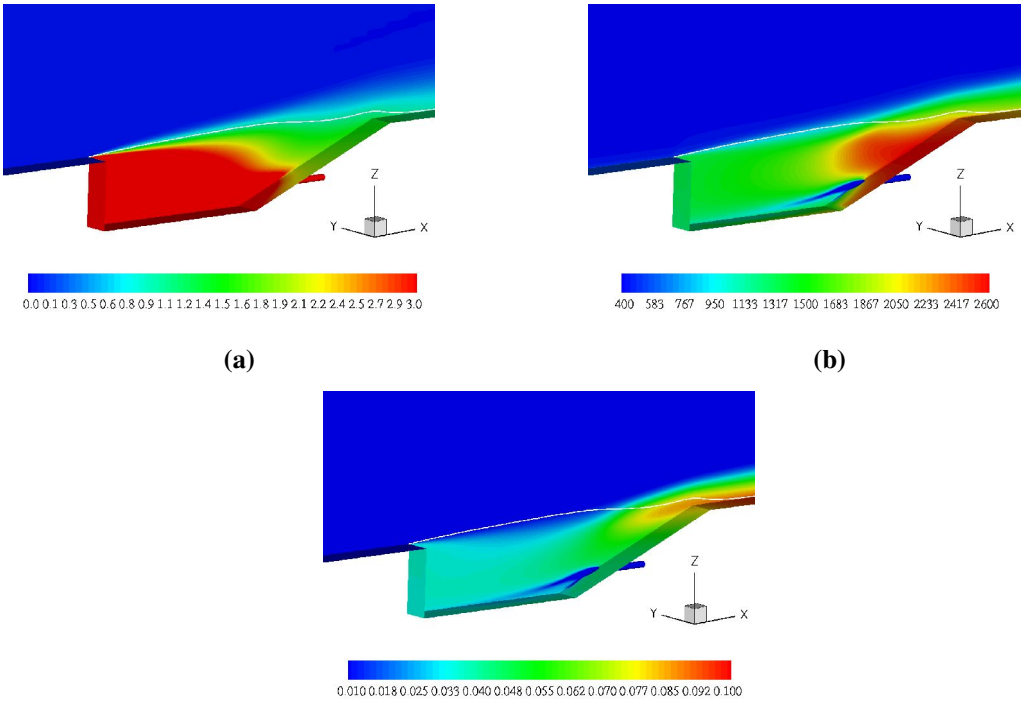

Figure 10. Contours of (a) local equivalence ratio, (b) temperature, and (c) CO_2 mass fraction for the 10X case.

In the above simulations, Sc_t was set at 0.5. As indicated in the previous section, Sc_t controls the turbulent mixing of fuel and air and its value is expected to have a strong impact on the turbulent combustion as well as the flame blowout prediction. In this study, this impact was demonstrated by considering three different Sc_ts for the fuel flowrate corresponding to the 4X case. Figures 11, 12, and 13 provide comparisons of local equivalence ratio, temperature, and CO_2 mass fraction contours for Sc_t of 0.3, 0.5, and 1.0. The extent of mixing of fuel and air is best expressed by the local equivalence ratio contour (Fig. 11). At Sc_t=0.3 (Fig. 11(a)), fuel and air mixing is very extensive and the stoichiometric line spans the center region of the cavity. The flow becomes fuel-rich only in a region very close to the cavity floor. As Sc_t is increased from 0.3 to 0.5, it seems that the fuel and air mixing slows down (Fig. 11(b)). The fuel-rich region near the cavity floor becomes thicker and it expands to the front wall of the cavity. As Sc_t is further increased to 1.0 (Fig. 11(c)), the mixing of fuel and air becomes less efficient. The fuel-rich region expands to the cavity center and pushes the stoichiometric line upward to near the freestream at the top of the cavity. From Fig. 11, the mixing extent of fuel and air is found to be related to the size of the red fuel-rich region. The larger the red region, the poorer the mixing of fuel and air.

Figure 12 shows the temperature contours for three different Sc_ts. At Sc_t=0.3, the enhanced mixing of fuel and air results in strong combustion across most of the cavity region, as seen in Fig. 12(a). The corresponding flame temperature reaches above 2600 K. As Sc_t is increased from 0.3 to 0.5, combustion becomes weaker and flame region size shrinks, due to the reduced mixing of fuel and air. At Sc_t=1.0 (12(c)), the front half of the cavity is flooded with fuel and the flow temperature in the recirculation zone is reduced significantly. Although the flame is sustained, it is pushed to a small region near the injector and the peak temperature is reduced to about 2000 K.

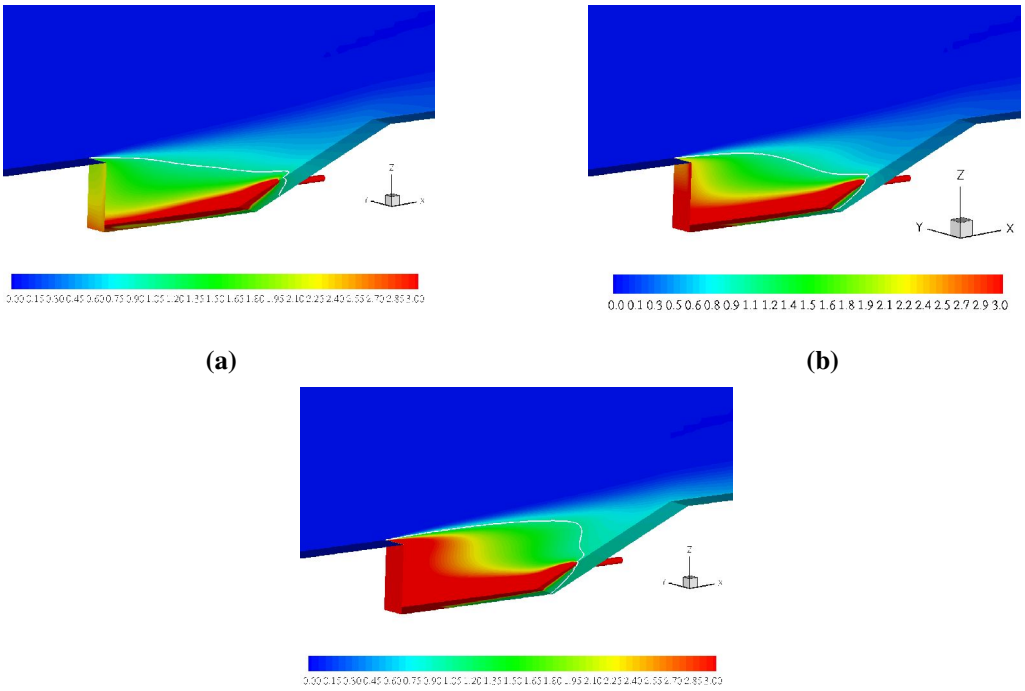

(a) **(b)**

(c)

Figure 11. Local equivalence ratio contours for Sc_t numbers of (a) 0.3, (b) 0.5, and (c) 1.0

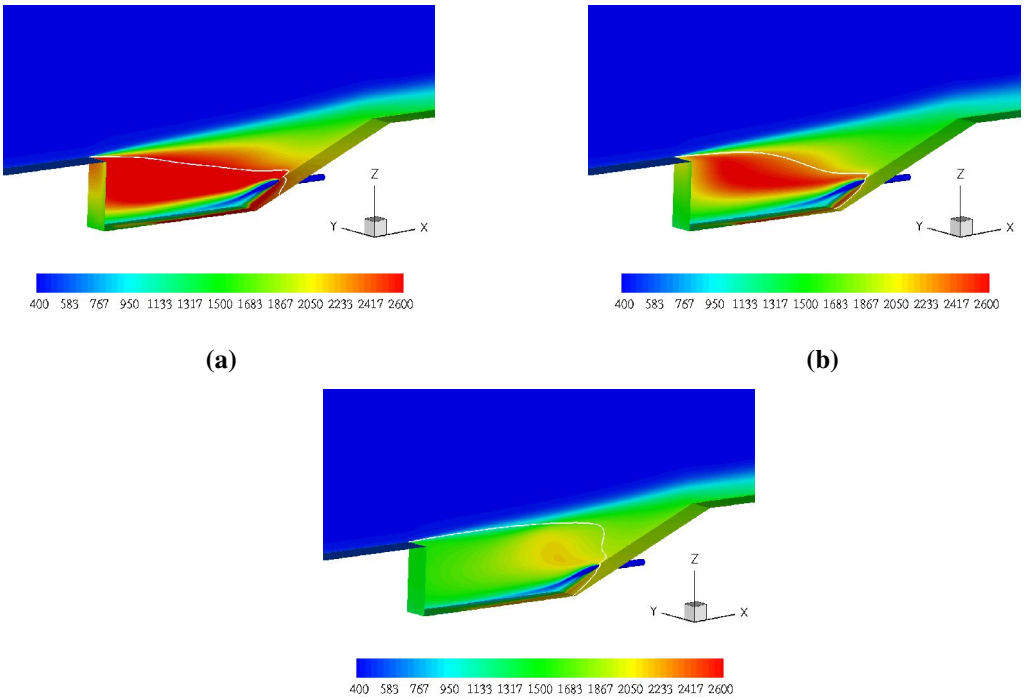

(a) **(b)**

(c)

Figure 12. Temperature contours for Sc_t numbers of (a) 0.3, (b) 0.5, and (c) 1.0

Figure 13 shows the CO_2 mass fraction contours for three different Sc_ts. As indicated before, a high flame temperature implies strong dissociation of CO_2 into CO. As a result, a relatively small quantity of CO_2 is found in the cavity region at Sc_t=0.3 (Fig. 13(a)), while a significant quantity of CO_2 is observed at Sc_t=1.0 in Fig. 13(c). The results shown in the these figures clearly demonstrate a strong sensitivity of combustion to Sc_t. In theory, the Sc_t for a specific application should be determined based on the calibration of experimental data. In reality, however, the rule of thumb is to set Sc_t=0.5. This value seems to work well for many applications involving scramjet engines.

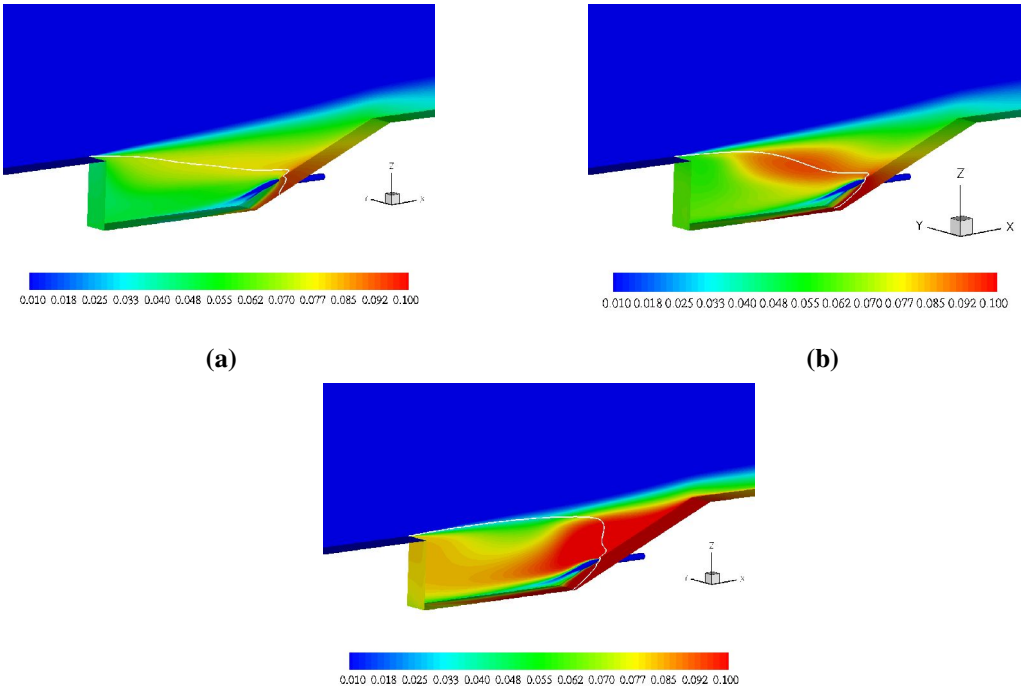

Figure 13. CO_2 mass fraction contours for Sc_t numbers of (a) 0.3, (b) 0.5, and (c) 1.0

C. Comparisons of results among the reduced mechanism and two global mechanisms

Currently, two most widely used ethylene combustion models to support the HyTech program are the 10-step quasi-global reaction mechanism developed by Singh and Jachimowski[14] and the 3-step global mechanism developed by researchers at AFRL.[13] These two models have been validated over a certain range of initial pressure, temperature, and equivalence ratio conditions based on the τ_{ign}. While these two models are very simple to apply, studies at AFRL and other organizations have shown great discrepancies between experiment measurements and the results obtained using these two models. To assess their validity in the present work on flame stability, these models were applied to simulate the same ARFL/PRA cavity combustor as that for the 15-step reduced mechanism. With the 10-step model, sustained combustion was not achieved, no matter what fuel flowrate was applied and what ignition approach was employed. With the 3-step model, sustained combustion was predicted only for the case with the fuel flowrate not smaller than that corresponding to the 4 X case and the Sc_t number not greater than 0.5. This implies that the flames predicted by the two global models blow out more easily than that predicted by the 15-step reduced model.

To understand the reason behind this phenomenon, the extinction residence time (τ_{ext}) in a PSR was calculated using the CHEMKIN software package for three different reaction models. The initial pressure and temperature in the PSR were chosen to be close to those in the core flow near the cavity region, and they were 0.5 atm and 325 K, respectively. Table 1 shows the comparison of the τ_{ext} at different φs for three reaction models. Overall the τ_{ext} predicted by the two global models are one or two orders of magnitude higher than that of the 15-step reduced model, which implies that the flame calculated from the 15-step reduced model is more difficult to blow out, due to the shorter extinction time. The large discrepancy in the τ_{ext} from different models should perhaps not be surprising because the two global models were developed to match the τ_{ign} only within a certain range of the initial conditions,

and they were NEVER intended to match the τ_{ext} in any condition. The extinction and the ignition processes are intrinsically different, in that a radical pool already exists for extinction, but it has to be built up in ignition. For predictions of blow-out, the flame already exists and extinction time is of more relevance than ignition time. Therefore, the two global models are inadequate for flame stability predictions.

Table 1. Comparison of τ_{ext} (sec.) for three kinetic mechanisms

	Kinetic mechanism		
φ	***3-step***	***10-step***	***15-step***
0.5	5.74E-02	3.05E-02	6.12E-04
1.0	2.87E-03	3.37E-03	7.19E-05
2.0	1.35E-03	1.94E-03	3.19E-04

Regarding the reason why the 10-step model failed to predict sustained combustion, the speculation is that the τ_{ext} from the 10-step mechanism is longer than those of other models, as seen in Table 1 for the region most favorable for flame formation. The local equivalence ratio in this region is normally around 1.0 or slightly higher, as shown in the previous figures. Another possible reason is that the 10-step model contains several additional radical species (OH, H, and O) than the 3-step model. As a result, the heat release and temperature predicted by the 10-step model are usually lower and flameholding is more difficult.

Even when sustained combustion is achieved, the flame structures predicted by different models may be different. Figures 14 and 15 show comparisons of local equivalence ratio and temperature contours between the reduced and 3-step models for Sc_t=0.5 and the fuel flowrate corresponding to the 5X case. While the local equivalence ratio contours (Fig. 14) predicted by the two models are very similar, their temperature contours (Fig. 15) are quite different. The flame predicted by the 3-step model is seen to extend much closer to the cavity front wall than that from the reduced model. In addition, the flame peak temperature predicted by the 3-step model is also higher. One major reason for this is the absence of radical species in the 3-step model. The energy consumed in radical formation is higher than the energy released in radical combination. Neglecting radical results in an over-prediction of the overall energy release in the flow and flame temperature. In addition, the 3-step model is only valid over a narrow range of conditions. Calculations made outside of these validation conditions may incur significant errors in the results. For example, CHEMKIN was used to calculate the τ_{ign} over a range of pressures and equivalence ratios. Both the 3-step and 10-step models predicted τ_{ign} that are at least an order of magnitude shorter than that from the detailed kinetic mechanism, once the temperature dropped below 1200 K. A short τ_{ign} implies enhanced combustion. Based on the above analysis, the 15-step reduced kinetic mechanism is preferred for ethylene combustion simulations because this model has been validated for many parameters such as the τ_{ign}, τ_{ext}, laminar flame speed, etc. over a wide range of flow conditions.

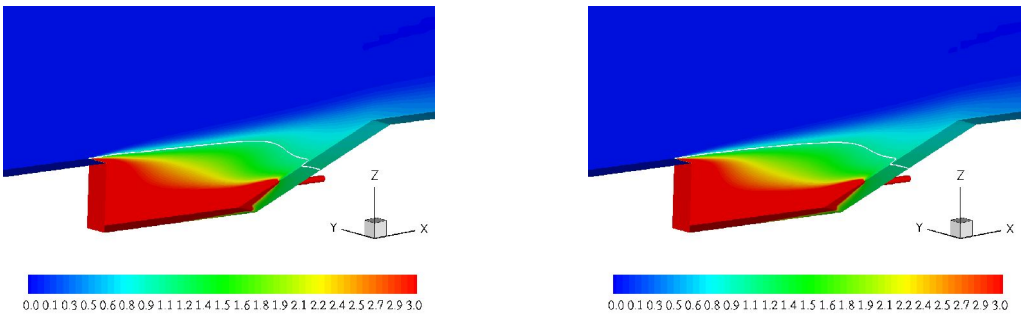

(a) **(b)**

Figure 14. Local equivalence ratio contours for (a) the reduced kinetic mechanism and (b) 3-step global mechanism.

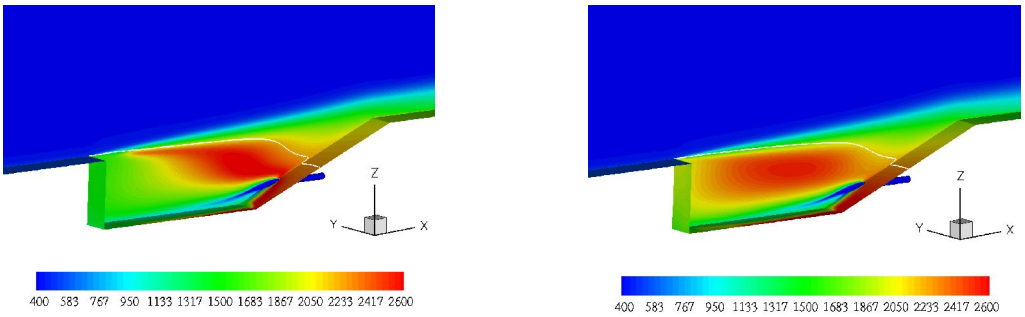

(a) **(b)**

Figure 15. Temperature contours for (a) the reduced kinetic mechanism and (b) 3-step global mechanism.

V. Conclusions

The VULCAN code along with a reduced chemical kinetic mechanism for ethylene oxidation has been applied to model the AFRL/PRA cavity combustor and predict cavity-stabilized flames at selected test run conditions. Several fuel flowrates have been considered, and combustion in the cavity involves fuel-lean as well as fuel-rich conditions. The predicted fuel flowrate at the lean blowout condition seems to match the experimental data. By considering several cases with different Sc_ts, the cavity combustion has been found to be sensitive to Sc_t. A value of 0.5 for Sc_t appears to be adequate for the present cavity combustor. To demonstrate the importance of using the reduced kinetic mechanism, two widely-used global kinetic models have been applied to simulate the present cavity combustor and they have been found to be inadequate for applications involving flame stability prediction. Because the 15-step reduced kinetic mechanism has been validated for many parameters over a wide range of flow conditions, it is preferred for ethylene combustion simulations.

Acknowledgments

This study was supported by USAF Contract FA8650-05-M-2616 and monitored by Dr. Skip Williams. The computational resources were provided by the Department of Defense High Performance Computing Centers. The work at Princeton University was, in addition, supported by the Air Force Office of Scientific Research under the technical management of Dr. Julian M. Tishkoff. The authors would also like to thank Dr. Kuang-Yu Hsu of ISSI, Inc. for technical insight and helpful discussion for the experimental data, and Dr. Robert Baurle of NASA Langley Research Center for guidance on the implementation of the reduced kinetic mechanisms into the VULCAN code.

References

[1] Mercier, R. A., and Ronald, T. M. F., "Hypersonic Technology (HyTech) Program Overview," AIAA Paper 98-1566, 1998.

[2] Mathur, T., Gruber, M., Jackson, K., Donbar, J., Donaldson, W., and Jackson, T., "Supersonic Combustion Experiments with a Cavity-Based Fuel Injector," Journal of Propulsion and Power, Vol. 17, pp. 1305-1312, 2001.

[3] Gruber, M. R., Donbar, J. M., Carter, C. D., and Hsu, K. Y., "Mixing and Combustion Studies Using Cavity-Based Flameholders in Supersonic Flow," Proceedings of International Society of Air-Breathing Engines, ISABE 2003-1204, 2003.

[4] Rasmussen, C. C., Driscoll, J. F., Hsu, K. Y., Donbar, J. M., Gruber, M. R., and Carter, C. D., "Stability Limits of Cavity-Stabilized Flames in Supersonic Flow," Proceedings of Combustion Institute, Vol. 30, pp. 2825-2833, 2005.

[5] Lu, T. and Law, C. K., "A Directed Relation Graph Method for Mechanism Reduction," Accepted for publication in Proceedings of the Combustion Institute, Vol. 30., 2005.

[6] White, J. A., and Morrison, J. H., "A Pseudo-Temporal Multi-Grid Relaxation Scheme for Solving the Parabolized Navier-Stokes Equations," AIAA Paper 99-3360, 1999.

[7] Zsely, I. G. and Turanyi, T., Chem. Phys., Vol. 5, pp. 3622-3631, 2003.

[8] Qin, Z., Lissianski, V. V., Yang, H., Gardiner, W. C., Davis, S. G., and Wang, H., Proc. Combust. Inst., Vol. 28, pp. 1663-1669, 2000.

[9] Chidambaram, N., Dash, S. M., and Kenzakowski, D. C., "Scalar Variance Transport in the Turbulence Modeling of Propulsive Jets," AIAA Paper 99-0235, 1999.

[10] Guo, Y. , He, G., and Hsu, A. T., "The Development of a Variable Schmidt Number Model for Jet-in-Crossflows Using Genetic Algorithms," AIAA Paper 99-0671, 1999.

[11] Baurle, R. A., Alexopoulos, G. A., and Hassan, H. A., "Analysis of Supersonic Combustors with Swept Ramp Injectors," Journal of Propulsion and Power, Vol. 13, pp. 327-328, 1997.

[12] Baurle, R. A. and Eklund, D. R., "Analysis of Dual-Mode Hydrocarbon Scramjet Operation at Mach 4-6.5," Journal of Propulsion and Power, Vol. 18, pp. 990-1002, 2002.

[13] Eklund, D. R., Baurle, R. A., and Gruber, M. R., "Computational Study of a Supersonic Combustor Fueled by an Aerodynamic Ramp Injector," AIAA Paper 2001-0379, 2001.

[14] Singh, D. J. and Jachimowski, C. J., "Qusiglobal Reaction Model for Ethylene Combustion," AIAA Journal, Vol. 32, pp. 213-216, 1994.